Eur. Phys. J. A **6**, 257–268 (1999)

THE EUROPEAN PHYSICAL JOURNAL A

Coincidence Doppler shift lifetime measurements in ^{73,74}Se and ^{74}Br using the EUROBALL Cluster cube array

R. Loritz[1], O. Iordanov[1], E. Galindo[1], A. Jungclaus[1], D. Kast[1], K. P. Lieb[1], C. Teich[1], F. Cristancho[1,2], Ch. Ender[3], T. Härtlein[3], F. Köck[3], D. Schwalm[3]

[1] II. Physikalisches Institut, Universität Göttingen, Bunsenstrasse 7-9, 37073 Göttingen, Germany
[2] Universidad Nacional de Colombia, Bogotá D. C., Colombia
[3] Max-Planck-Institut für Kernphysik, 69029 Heidelberg, Germany

Received: 2 July 1999
Communicated by B. Povh

Abstract. Subpicosecond lifetimes of high spin states in the rotational nuclei ^{73}Se, ^{74}Se and ^{74}Br have been measured using the ^{58}Ni + ^{19}F compound reaction and the Doppler Shift Attenuation method. Six EUROBALL Cluster detectors arranged in cube geometry allowed us to select the relevant transitions in $\gamma\gamma$ coincidence mode. The high counting statistics achieved in this setup also facilitated the determination of average sidefeeding times, which were found to agree rather well with the results of Monte-Carlo calculations of the particle and γ-ray evaporation process. The deduced quadrupole strengths and deformations are compared with the results of previous measurements and the predictions of Cranked Shell Model calculations. In ^{74}Br, a large and constant prolate deformation of β_2=0.37(1) was found for the presumed 4^+ and 3^- two-quasiparticle bands.

PACS. 23.20.Js Multipole matrix elements – 23.20.Lv Gamma transitions and level energies – 24.60.Dr Statistical compound-nucleus reactions – 27.50.+e $59 \leq A \leq 89$

1 Introduction

Nuclear lifetimes are among the most sensitive quantities for testing nuclear models. In the strongly deformed nuclei of the mass A = 80 region, rapid changes of the quadrupole deformation as function of spin and proton and neutron numbers have given important insights into the evolution of the quadrupole collectivity as predicted by the single-particle Nilsson and Cranked Shell Model [1]. A rich variety of structure effects has been encountered in this mass region, such as the occurrence of very large quadrupole moments and even superdeformed bands [2–4], interference of strongly and weakly deformed structures at low spins [5], changes of the triaxiality parameter γ giving rise to prolate and oblate rotational bands (e.g. in $^{69-72}$Se [5–7], $^{76-80}$Kr [8–10]), variations of the quadrupole deformation due to high-j particle alignments, and, as observed most recently, magnetic rotation in the $^{82-84}$Rb isotopes [11].

In the nuclei ^{73,74}Se and ^{74}Br for which subpicosecond lifetime measurements were carried out in the present work, previous results of lifetime measurements have been reported [12,13,15,21–23]. The motivations to extend these data and to try to improve the Doppler Shift Attenuation (DSA) measurements were two-fold: The previous experiments were performed with set-ups containing a small number of (mainly Compton-suppressed) Ge detectors. Only in very few cases, the Doppler broadened lineshapes analyzed could be selected in $\gamma\gamma$-coincidence mode allowing to remove unwanted and in some cases even Doppler broadened contaminant lines. More severe is the lack of knowledge of sidefeeding times, which play an important role in the determination of the short lifetimes to be associated with highly deformed bands in this mass region. Indeed, there are only few nuclei and reactions in the A = 80 region for which reliable sidefeeding times τ_{SF} have been measured so far [16–18]. In many cases the limited counting statistics of the Doppler broadened lineshapes only permitted to establish a correlation between the state lifetime τ and the average sidefeeding time τ_{SF}, leaving ambiguous the individual values of them. By using a set-up of six EUROBALL cluster detectors in a cube geometry [19,20], i.e. a total of 42 Ge detectors, we hoped to be able to remedy both problems. The high efficiency of these detectors and the large solid angle covered in the cube arrangement provided for the possibility to observe, in $\gamma\gamma$ coincidence mode, Doppler broadened lineshapes with high counting statistics.

Correspondence to: Klaus-Peter Lieb

Details of the experimental arrangement and data analysis will be presented in Sect. 2, while the deduced lifetimes and sidefeeding times will be summarized in Sect. 3. A short account of the deduced transition strengths follows in Sect. 4.

2 Experiment and analysis

Excited states in the evaporation residues ^{73}Se, ^{74}Se and ^{74}Br were populated by bombarding ^{58}Ni with a 2.2 particle-nA 70-MeV ^{19}F-ion beam provided by the MP tandem accelerator of the Max-Planck-Institut für Kernphysik, Heidelberg. These three nuclei are fed in the strong 3pn, 3p and 2pn evaporation channels [12–15, 21–24]. The target was a 1.0 mg/cm^2 nickel layer enriched in ^{58}Ni to 99% and deposited onto a 12 μm thick gold foil. The target was positioned, at 45° to the beam, in the center of a setup of six EUROBALL cluster detectors arranged in cube geometry (see Fig. 1). Each cluster detector [19] houses seven individually encapsulated Ge crystals of 60% efficiency each; the energy resolution of the Ge detectors was 2.4 keV at 1.33 MeV. The central modules of four clusters, i.e. the detectors A7, B7, D7, F7 in Fig. 1, were located at 45° and 135° to the beam axis, while the two remaining clusters (C, E) were positioned at 90° to the beam, above and below the plane formed by the beam and the four central modules of the clusters A, B, D, F. The distance from the target to these center Ge detectors was about 11 cm. This close geometry did not allow us to use the BGO Compton suppression shields of the clusters, but at least the "backcatcher" BGO crystals located behind the Ge segments served for partial Compton suppression [19]. The number of two-fold $\gamma\gamma$ coincidence events at the various angles ranged from 6.5x10^8 to 11.4x10^8.

The symmetry of the detector arrangement within each of the clusters A, B, D and F and their symmetry with respect to both sides of the beam and in the forward and backward directions was exploited to gain high counting statistics and symmetric Doppler broadened lineshapes by summing the spectra of individual modules having the same polar angle Θ with respect to the beam direction. The modules contributing to the six angular groups used in the lineshape analysis to produce the "look" spectra are given in Table 1. The symmetry of the setup also enabled us to identify those weak contaminants which were still not fully removed in the coincidence data. These contaminants as well as γ-ray multiplets are a consequence of the high line density in the spectra, the large number of nuclei populated, and the similarity in moment-of-inertia parameters in these neighboring nuclei giving rise to closely lying transitions. Multiplets were identified by comparing the spectra in the forward and backward detectors and looking for peaks either not depending in their positions on the detection angle or their shifted parts being symmetric around $\Theta = 90°$.

In the analysis of the $\gamma\gamma$ coincidence spectra, Doppler broadened lineshapes were deduced from the "look" spectra observed in each of the six groups of modules listed in Table 1. The gates were set on lines in all "non-neighbour"

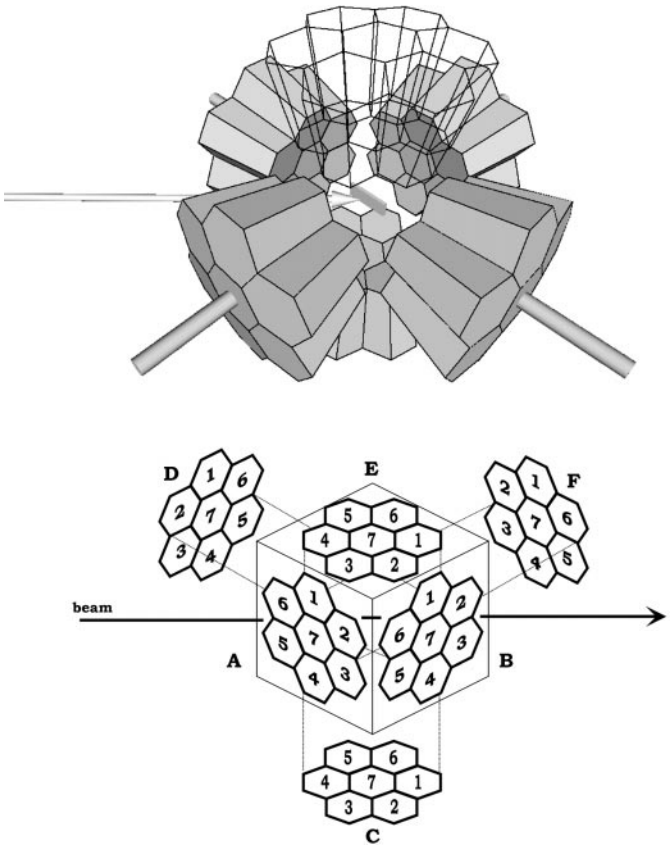

Fig. 1. Cluster cube arrangement used in the present experiment

Table 1. Cluster modules contributing to the six angular groups used in the lineshape analysis

Cluster	module number	Θ(°)
B, F	B1, B4, F1, F4	52
	B2, B3, F5, F6	24
	B5, B6, F2, F3	71
A, D	A1, A4, D1, D4	128
	A5, A6, D2, D3	156
	A2, A3, D5, D6	109

Ge crystals, i.e. in all the modules of those clusters not containing the "look" detector and in all the modules in the "look" cluster not adjacent to the "look" detector firing in the particular event. As an example we illustrate in Fig. 2 lineshapes of the strong 967 keV $8^+ \rightarrow 6^+$ transition within the ground band of ^{74}Se, taken at the six different "look" angles of the clusters A, B, D and F. One clearly notes the different line broadenings as a result of the $\cos\Theta$ dependence of the Doppler effect. It is important to note that the gates were set on transitions further down the cascades. Consequently all these lineshapes are affected by the lifetimes and sidefeeding times of the upper transitions within the bands.

For analyzing the lineshapes we used the programs DESASTOP and DOPPIDIF developed by Winter [25]. These programs account for the energy loss of the beam

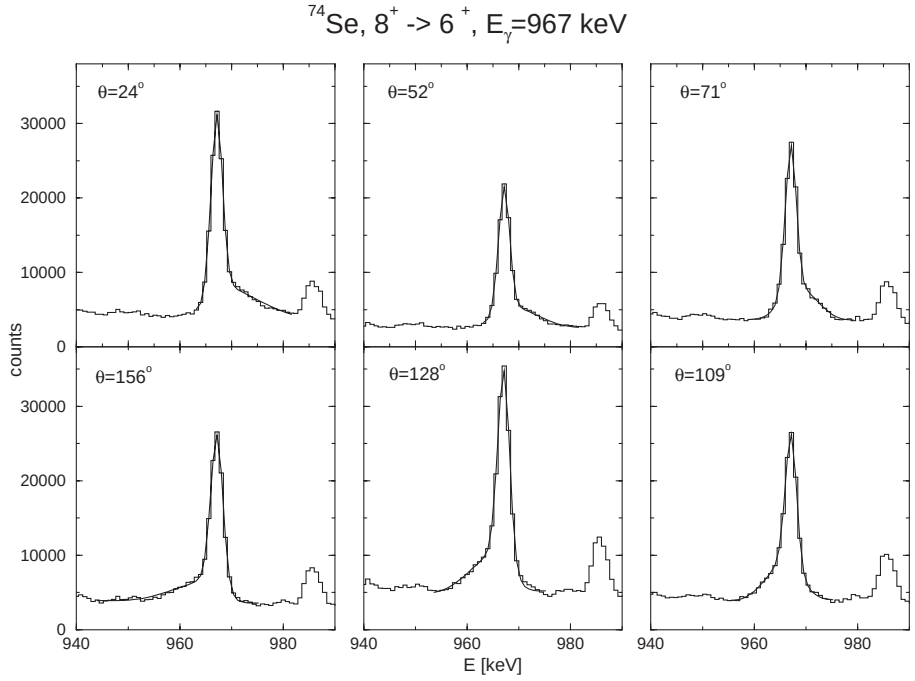

Fig. 2. Doppler broadened lineshapes of the 967 keV $8^+ \rightarrow 6^+$ transition in ^{74}Se, measured at the angles indicated, in coincidence with the 868 keV $6^+ \rightarrow 4^+$ transition of the ground band

in the target, the energy and angular distributions of the recoils resulting from the kinematics of the particle evaporation process and the stopping power of the recoils in the target and stopper. The stopping power of the beam and of the recoils in the target and backing were treated according to Lindhard, Scharff and Schiøtt (electronic and nuclear stopping) [26]; the angular straggling of the recoils was Monte-Carlo simulated. For each level, the discrete feeding and side feeding intensities were evaluated from the spectra making use of the published level schemes [12–15,21–24]. Details of the fitting procedure have been described by Harder and collaborators [18] in their detailed study of rotational bands in ^{77}Rb. For each angle, the lineshapes were fitted individually and the deduced lifetime values were then averaged. As expected, the lineshapes at the most forward and backward angles (24°, 156°) are most sensitive to the fitting parameters, because the energy spread of the lineshapes is larger here as compared to angles of observation closer to 90°. In general, these lifetime values agreed very well with those obtained at 52° and 128°, but less with those deduced at 71° and 109° having the smallest Doppler effects and the largest uncertainties. The latter values were therefore not included in the final numbers, which are weighted average values.

3 Results

Figure 3 illustrates partial level schemes of the three nuclei, which exhibit the rotational bands, including the gating transitions and the feeding patterns relevant for the present study. The lineshapes within the strongly populated ground band in ^{74}Se turned out to be most sensitive and allowed for a separate determination of state lifetimes τ and sidefeeding times τ_{SF}. For that reason, we discuss these results first and infer from the resulting sidefeeding times the corresponding τ_{SF} values used in the analysis of the lineshapes observed in ^{73}Se and ^{74}Br.

3.1 Lifetimes and sidefeeding times in ^{74}Se

Measured and fitted lineshapes of transitions in the spin range 8^+ - 16^+ of the ground band of ^{74}Se taken at 52° are displayed in Fig. 4. In all cases the gate was the 868 keV $6^+ \rightarrow 4^+$ line. Due to the decreasing lifetime for increasing spin value, the Doppler shifted components of the lineshapes increase in intensity with increasing spin, while the unshifted components vanish. The discrete feedings from the positive-parity, odd-spin band (labeled band #1 in [14]) and another even-spin band (labeled band #3 in [14]) are very small and the corresponding feeder lines were not observed in the present work. The τ - τ_{SF} correlations deduced at 24° and 156° for the 1292 keV $14^+ \rightarrow 12^+$ transition are illustrated in Fig. 5, which also displays the dependence of the reduced χ^2 goodness-of-fit parameter on τ_{SF}. The analysis of both lineshapes gives consistent results for τ and τ_{SF}, but with rather large uncertainties: $\tau = 0.15(4)$ ps and $\tau_{SF} = 0.21(5)$ ps. It is well known that, for a given feeding pattern and in the case of strong sidefeeding intensity, the lineshape of the decay γ-ray is mainly sensitive to the sum $(\tau + \tau_{SF})$, but less to their individual values. Nonetheless, the good counting statistics and the fit of six lineshapes for each transition provided the possibility to disentangle the τ - τ_{SF} correlations in this band and to obtain reliable values for both τ and τ_{SF}.

The deduced lifetimes τ and sidefeeding times τ_{SF} in ^{74}Se are listed in Table 2a. The results of several previous DSA experiments using compound reactions induced

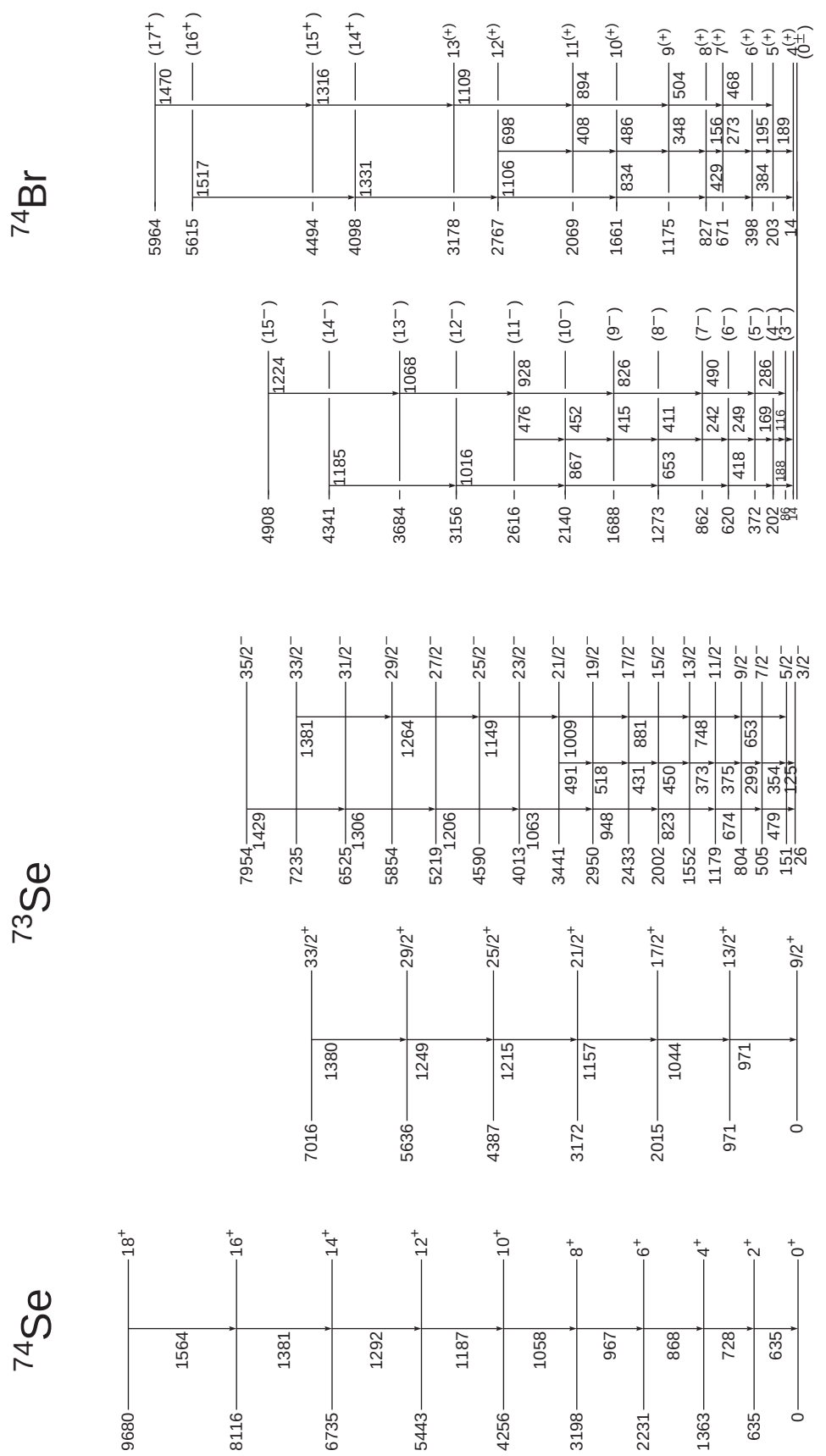

Fig. 3. Relevant level schemes and feeding patterns of the three nuclei ^{74}Se (a), ^{73}Se (b) and ^{74}Br (c) (from [14,12,24]) for which lifetimes were obtained in the present work

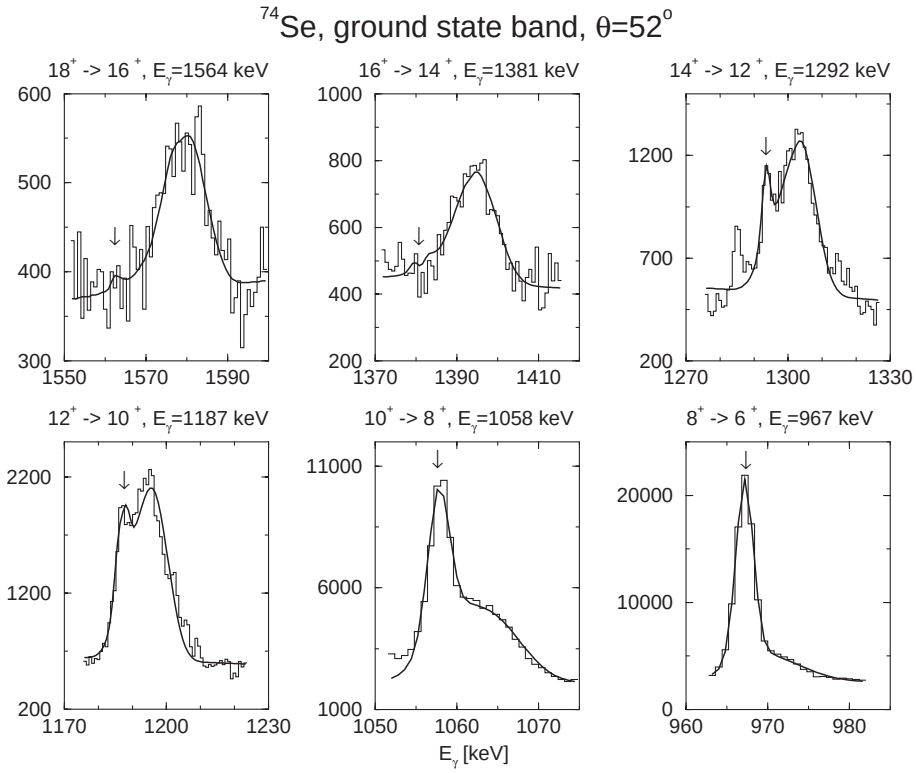

Fig. 4. Doppler broadened lineshapes of ground band transitions in ^{74}Se, measured at 52°

Table 2. Summary of (a) lifetimes τ and sidefeeding times τ_{SF} and of (b) transitional quadrupole moments $|Q_t|$ and deformations $|\beta_2|$ in ^{74}Se.

(a) Lifetimes and sidefeeding times[a]

				present work[a]				previous work			
				simultaneous fit		calc.[b]	fit[c]	[13]		[23]	
State E_x (keV)	I^π	E_γ (keV)	I_{SF} (%)	τ_{SF} (ps)	τ (ps)	τ_{SF} (ps)	τ (ps)	τ_{SF} (ps)	τ (ps)	τ_{SF} (ps)	τ (ps)
3198	8^+	967	18(2)	0.9(5)	0.43(4)	1.13	0.38(2/5)	0.1	0.80(15)	0.17	0.54(3)
4256	10^+	1058	13(2)	0.5(2)	0.22(2)	0.63	0.20(1/2)	< 0.1	0.40(10)	0.14	0.35(3)
5443	12^+	1187	43(3)	0.25(4)	0.10(2)	0.34	0.09(1/3)	< 0.1	0.24(5)	0.11	0.16(2)
6735	14^+	1292	62(3)	0.21(5)	0.15(4)	0.23	0.14(1/3)	< 0.1	0.26(6)	0.08	0.19(2)
8116	16^+	1381	49(5)	0.11(4)	0.10(2)	0.12	0.09(1/2)	< 0.1	< 0.23	0.05	0.18(5)[d]
9680	18^+	1564	-	-	0.17(2)[d]	-	-	-	-	-	-

a: Gate always on 868 keV transition
b: τ_{SF} calculated with GAMMAPACE
c: (statistical/systematic) error
d: Effective lifetime (not corrected for feeding)

(b) Transition probabilities and deformation parameters

State E_x (keV)	I^π	E_γ (keV)	branch (%)	τ[a] (ps)	B(E2) (W.u.)	Q_t (eb)	β_2
3198	8^+	967	100	0.38(5)	$138\binom{21}{16}$	$2.78\binom{20}{17}$	0.40(3)
4256	10^+	1058	100	0.20(2)	$167\binom{19}{15}$	$3.02\binom{16}{14}$	0.43(2)
5443	12^+	1187	100	0.09(3)	$106\binom{104}{52}$	$3.35\binom{75}{45}$	$0.48\binom{10}{6}$
6735	14^+	1292	100	0.14(3)	$62\binom{24}{16}$	$2.16\binom{28}{20}$	0.32(4)
8116	16^+	1381	100	0.09(2)	$88\binom{28}{18}$	$2.27\binom{30}{22}$	0.33(4)
9680	18^+	1564	100	≤ 0.19	≥ 25	≥ 1.14	≥ 0.17

a: Adopted lifetime

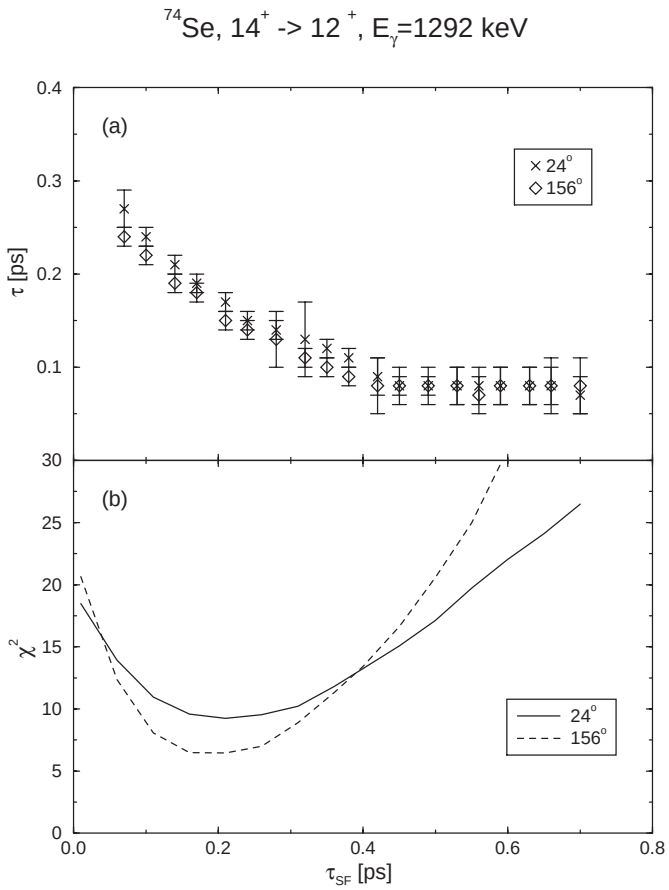

Fig. 5. (a) Correlations of the state lifetime τ of the 14^+ state in ^{74}Se and the average sidefeeding time τ_{SF}, at $\Theta = 24°$ and 156°. (b) Variation of the χ^2-parameter as function of the sidefeeding time τ_{SF}

by α-particles, ^{12}C, ^{16}O and ^{19}F projectiles are given for comparison in Columns 10 and 12 of Table 2a [23,27,28]. Evidently, the lifetime values scatter substantially due to the fact that the sidefeeding times adopted in the previous studies have been rather small (see Columns 9 and 11). A direct comparison of our work with the ^{58}Ni + ^{19}F study at 63 MeV by Cottle et al. illustrates this point. Due to the much shorter sidefeeding times adopted in [23], these lifetimes are considerably longer than ours. When inserting the shorter sidefeeding times adopted in the former work into the analysis of our data, we found very good agreement among their and our lifetime values. Although the smaller beam energy used in [23] will lead to somewhat shorter sidefeeding times, it results from the present work that the τ_{SF} values of Cottle et al. [23] are systematically too small by roughly a factor of two (see below).

The particle and gamma ray evaporation processes after heavy-ion fusion in the mass 80 region were modelled by means of the program GAMMAPACE, developed by Cristancho and Lieb [29] on the basis of the PACE code [30]. GAMMAPACE simulates the flux and time-evolution of the fusion-evaporation reaction into a given discrete state in the final nucleus considered and provides the distributions of the continuum γ-ray energies, multiplicities, multipolarities and sidefeeding times. The latter depend on, among other quantities, the electric quadrupole strengths of the continuum radiation which we evaluated from the average quadrupole deformation deduced from the lifetimes of the ground band of the final nucleus considered. Figure 6 compares the calculated and experimental average sidefeeding times τ_{SF} as function of the level spin I and excitation energy E_x of the yrast state, respectively. It is rewarding to see that the rather strong variation of τ_{SF} is well reproduced by the evaporation simulation. A similarly good agreement had been previously found by Galindo and Cristancho [31] in the case of the reaction ^{40}Ca(^{40}Ca,3p)^{77}Rb at E = 128 MeV for the sidefeeding times determined by Harder et al. [18]. As shown in Fig. 6, the strong dependence of the sidefeeding time on the excitation energy E_x or the level spin I is well reproduced by the fusion-evaporation calculations [18]. We refer to the previous papers [18,29,31] for further details of the calculations and the parameters used. The lifetimes deduced when adopting the calculated sidefeeding times are given in Column 8 of Table 2a. In order to distinguish between the purely statistical and the total errors of the lifetimes, both values are given. The total errors were estimated by using the formula

$$(\Delta\tau)_{total} = \sqrt{(\Delta\tau)^2_{stat} + (\Delta\tau)^2_{syst}} \qquad (1)$$

with the estimated systematic error

$$(\Delta\tau)_{syst} = 0.2 \cdot \tau_{SF} \cdot I_{SF} \qquad (2)$$

with I_{SF} being the relative sidefeeding intensity of the state.

3.2 Lifetimes in ^{73}Se

A total of 12 lifetimes and three lifetime limits for states in the positive and negative parity yrast bands of ^{73}Se sketched in Fig. 3b were obtained in this analysis. They are summarized in Table 3a. In both bands, we calculated the sidefeeding times τ_{SF} by means of GAMMAPACE and inserted the values into the lineshape analyses. Fig. 7 illustrates the lineshapes, which refer to the ΔI = 2 positive parity yrast band in the spin range $17/2^+$ - $33/2^+$ taken at 156° (including the three non-Doppler shifted contaminant lines at 1368 keV, 1240 keV and 1150 keV). As a consequence of the calculated longer sidefeeding times τ_{SF} (see Column 6 of Table 3a), we again face a discrepancy between the shorter lifetime values of the present work (Column 6) and the generally larger values recently obtained by Mukherjee et al. [12] in the reaction ^{51}V(^{29}Si,αpn) and listed in Column 8 of Table 3a. Unfortunately, this latter work does not quote the assumed sidefeeding times. The results of a previous DSA study by Seiffert et al. [21] are in better agreement with the present ones.

Table 3. Summary of (a) lifetimes τ and sidefeeding times τ_{SF} and of (b) transitional quadrupole moments Q_t and deformations β_2 in ^{73}Se

(a) Lifetimes and sidefeeding times

					present work				previous work	
					simultaneous fit		calc.[a]	fit[b]	[12]	[21]
State		E_γ	I_{SF}	Gate	τ_{SF}	τ	τ_{SF}	τ	τ	τ
E_x (keV)	I^π	(keV)	(%)	(keV)	(ps)	(ps)	(ps)	(ps)	(ps)	(ps)
2015	$17/2^+$	1044	40(2)	971	-	-	0.66	0.26(6)	0.53(7)	0.45(10)
3172	$21/2^+$	1157	53(5)	1044	0.30(7)	0.27(3)	0.40	0.20(2/5)	0.26(6)	0.2(1)
4387	$25/2^+$	1215	51(7)	971	0.10(3)	0.11(2)	0.23	0.09(1/3)	0.09(2)	-
5636	$29/2^+$	1249	39(11)	971	0.06(4)	0.22(2)	0.12	0.17(2/2)	0.16(4)	-
7016	$33/2^+$	1380	-	971	-	-	-	0.13(1)[c]	0.31(9)	-
2433	$17/2^-$	881	49(4)	d	-	-	0.89	0.63(6/11)	0.69(13)	0.4(2)
2950	$19/2^-$	948	40(5)	d	-	-	0.82	0.29(4/8)	0.52(10)	0.4(2)
3441	$21/2^-$	1009	18(5)	d	-	-	0.61	0.18(2/3)	0.45(5)	0.30(15)
4013	$23/2^-$	1063	21(4)	d	-	-	0.43	0.15(1/2)	0.47(6)	0.5(3)
4590	$25/2^-$	1149	42(7)	e	-	-	0.30	0.09(1/3)	0.27(4)	-
5219	$27/2^-$	1206	43(6)	e	-	-	0.20	0.10(1/2)	0.15(2)	-
5854	$29/2^-$	1264	51(2)	f	-	-	0.13	0.08(1/2)	0.12(2)	-
6525	$31/2^-$	1306	62(9)	d	-	-	0.10	0.10(2/2)	0.19(3)	-
7235	$33/2^-$	1381	-	d	-	-	-	0.20(2)[c]	0.23(4)	-
7954	$35/2^-$	1429	-	d	-	-	-	0.34(3)[c]	0.17(4)	-

a: τ_{SF} calculated with GAMMAPACE
b: (statistical/systematic) error
c: Effective lifetime (not corrected for feeding)
d: Gates: 125, 354, 479, 748 keV
e: Gates: 125, 479, 748 keV
f: Gates: 125, 354, 479 keV

(b) Transition probabilities and deformation parameters

State		E_γ	branch	τ^a	B(E2)	Q_t	β_2
E_x (keV)	I^π	(keV)	(%)	(ps)	(W.u.)	(eb)	
2015	$17/2^+$	1044	100	0.26(6)	$137\binom{41}{26}$	$3.07\binom{43}{30}$	$0.44\binom{6}{4}$
3172	$21/2^+$	1157	100	0.20(5)	$107\binom{36}{21}$	$2.57\binom{40}{27}$	$0.37\binom{5}{4}$
4387	$25/2^+$	1215	100	0.09(3)	$186\binom{93}{46}$	$3.30\binom{74}{44}$	$0.47\binom{10}{6}$
5636	$29/2^+$	1249	100	0.17(2)	$85\binom{11}{9}$	$2.20\binom{14}{12}$	0.32(2)
7016	$33/2^+$	1380	100	< 0.14	> 68	> 1.80	> 0.25
2433	$17/2^-$	881	70	0.63(11)	$93\binom{20}{14}$	$2.53\binom{25}{20}$	0.37(3)
2950	$19/2^-$	948	60	0.29(8)	$120\binom{46}{26}$	$2.78\binom{49}{32}$	$0.40\binom{7}{4}$
3441	$21/2^-$	1009	100	0.18(3)	$236\binom{47}{34}$	$3.83\binom{37}{28}$	$0.54\binom{5}{4}$
4013	$23/2^-$	1063	100	0.15(2)	$217\binom{33}{26}$	$3.62\binom{27}{22}$	$0.51\binom{4}{3}$
4590	$25/2^-$	1149	100	0.09(3)	$245\binom{123}{61}$	$3.80\binom{85}{51}$	$0.54\binom{11}{7}$
5219	$27/2^-$	1206	100	0.10(2)	$173\binom{43}{29}$	$3.16\binom{37}{28}$	$0.45\binom{5}{4}$
5854	$29/2^-$	1264	100	0.08(2)	$171\binom{57}{34}$	$3.12\binom{48}{33}$	$0.45\binom{6}{4}$
6525	$31/2^-$	1306	100	0.10(2)	$116\binom{29}{19}$	$2.55\binom{30}{22}$	$0.37\binom{4}{3}$
7230	$33/2^-$	1381	100	< 0.22	> 36	> 1.42	> 0.20
7954	$35/2^-$	1428	100	< 0.37	> 18	> 1.00	> 0.15

a: Adopted lifetime

3.3 Lifetimes in ^{74}Br

As shown in Fig. 3, the high-spin level scheme of the odd-odd nucleus ^{74}Br is made up by yrast bands having ΔI = 2 E2 cross-over and parallel ΔI = 1 transitions. Due to this fact, setting coincidence gates on high-intensity transitions at the bottom of the bands sometimes led to overlapping Doppler broadened lineshapes of transitions being close in energy. On the other hand, the limited counting statistics of Doppler broadened lines obtained when gating on higher lying transitions did not allow us to achieve independent fits for the sidefeeding and level lifetimes. For that reason and in view of the supporting evidence from the ^{73,74}Se analysis, the respective sidefeed-

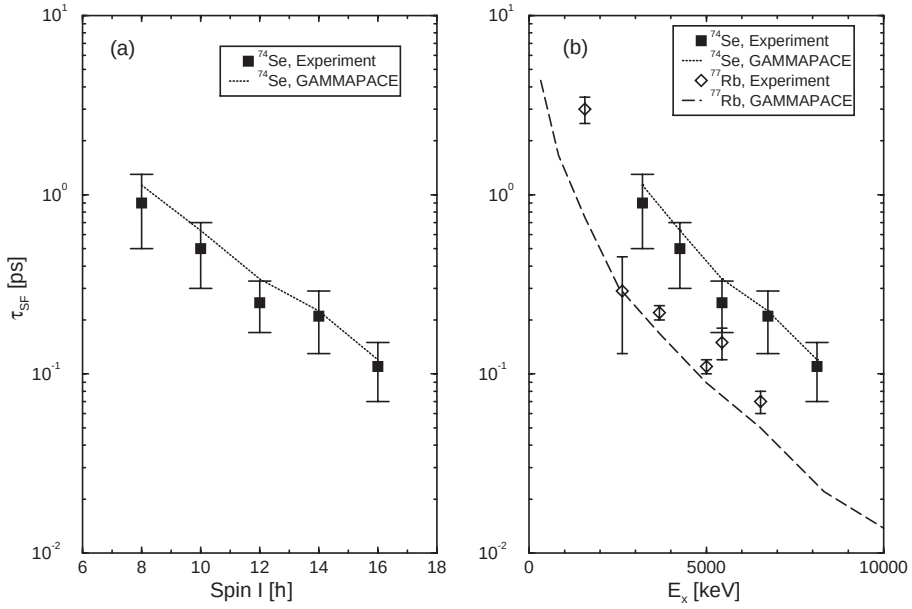

Fig. 6. Values of the average sidefeeding time τ_{SF} in ^{74}Se plotted as function of the level spin I (a) or the excitation energy E_x (b). The results of Monte-Carlo simulations using the code GAMMAPACE are also inserted as well as measured and calculated sidefeeding times in ^{77}Rb [17,27]

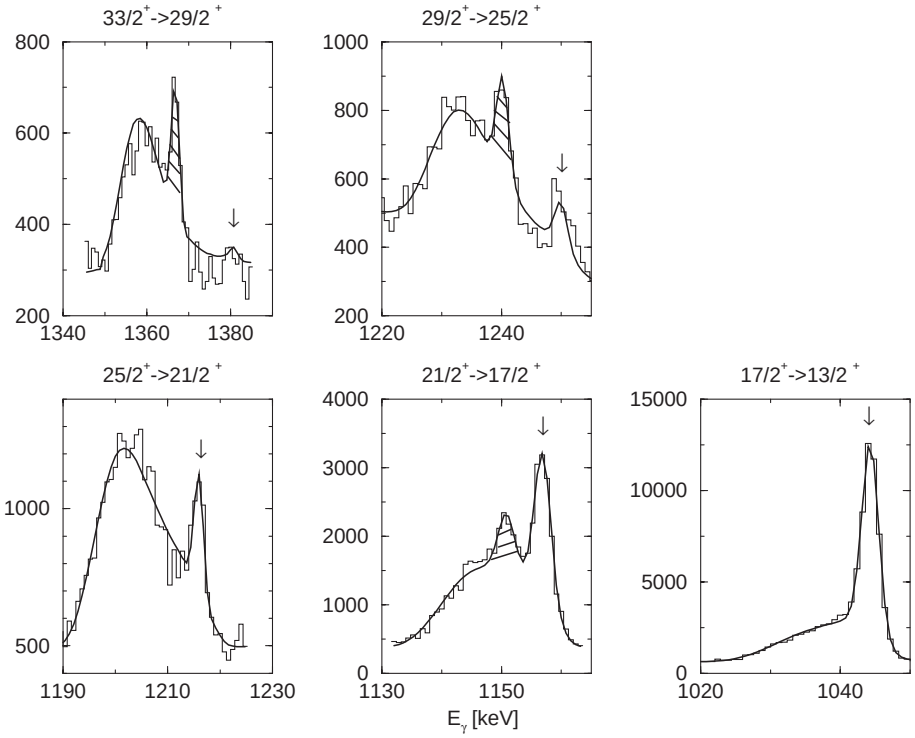

Fig. 7. Measured and fitted Doppler broadened lineshapes of transitions within the decoupled $g_{9/2}$ yrast band in ^{73}Se. The deduced lifetimes are summarized in Table 3. The hatched peaks are contaminant lines

ing times were calculated by means of GAMMAPACE and inserted in the analysis. Figs. 8a and b illustrate measured and fitted Doppler broadened lineshapes of the 894 keV $11^{(+)} \rightarrow 9^{(+)}$ and 1068 keV $(13^-) \rightarrow (11^-)$ transitions in ^{74}Br recorded at $\Theta = 24°$, 52°, 128° and 156° to the beam.

Table 4a summarizes the calculated sidefeeding times and deduced lifetimes. In comparison with the previous recoil distance experiment by Holcomb et al. [15], we notice good agreement and much improved precision of the present DSA work, a consequence of the high efficiency of the cluster set-up and the careful consideration of sidefeeding times. Besides the effective lifetimes of the 4341 keV 14^-, 4909 keV 15^-, 5615 keV 16^+ and 5962 keV 18^+ states, a total of eight level lifetimes were measured in ^{74}Br leading to collective E2 strengths of 90 - 140 W.u. and an average deformation parameter of $\beta_2 = 0.37$ for both bands to be further discussed in Sect. 4.

Table 4. Summary of (a) lifetimes τ and sidefeeding times τ_{SF} and of (b) transitional quadrupole moments Q_t and deformations β_2 in ^{74}Br.

(a) Lifetimes and sidefeeding times

				present work			previous work
					calc.[a]	fit[b]	[15]
State		E_γ	I_{SF}	Gate	τ_{SF}	τ	τ
E_x (keV)	I^π	(keV)	(%)	(keV)	(ps)	(ps)	(ps)
2616	(11^-)	928	31	d	0.50	0.42(1/3)	0.54(12)
3156	(12^-)	1016	25	653,867	0.29	0.41(7/7)	< 0.50
3684	(13^-)	1068	38	e	0.24	0.25(1/2)	< 0.53
4341	(14^-)	1185	-	d	-	0.20(1)[c]	-
4908	(15^-)	1224	-	f	-	0.19(1)[c]	-
2069	$11^{(+)}$	894	27	348	0.44	0.47(3/4)	0.45(15)
2767	$12^{(+)}$	1106	54	834	0.22	0.21(1/3)	0.23(6)
3178	$13^{(+)}$	1109	31	348	0.21	0.20(1/2)	0.21(5)
4098	(14^+)	1331	21	834	0.11	0.15(1/1)	< 0.19
4494	(15^+)	1316	57	348	0.12	0.08(1/2)	< 0.24
5615	(16^+)	1517	-	429	-	0.20(3)[c]	-
5964	(17^+)	1470	-	g	-	0.18(2)[c]	-

a: τ_{SF} calculated with GAMMAPACE
b: (statistical/systematic) error
c: Effective lifetime (not corrected for feeding)
d: Gates: 116, 169, 418, 490, 826 keV
e: Gates: 116, 169, 418, 490 keV
f: Gates: 116, 169, 826 keV
g: Gates: 195, 273, 348, 383, 407, 429, 894 keV

(b) Transition probabilities and deformation parameters

State		E_γ	branch	τ^a	B(E2)	Q_t^b	β_2
E_x (keV)	I^π	(keV)	(%)	(ps)	(W.u.)	(eb)	
2616	(11^-)	928	75(1)	0.42(3)	114(9)	2.72(11)	0.38(2)
3156	(12^-)	1016	100	0.41(5)	99(13)	$2.49\binom{24}{19}$	0.35(2)
3684	(13^-)	1068	100	0.25(1)	126(10)	2.76(11)	0.39(2)
4341	(14^-)	1185	100	< 0.22	> 85	> 2.25	> 0.32
4908	(15^-)	1224	100	< 0.20	> 80	> 2.15	> 0.30
2069	$11^{(+)}$	894	63(1)	0.47(5)	103(12)	2.78(16)	0.39(2)
2767	$12^{(+)}$	1106	79(3)	0.21(3)	100(12)	2.65(15)	0.37(2)
3178	$13^{(+)}$	1109	100	0.20(2)	131(14)	2.96(15)	0.41(2)
4098	(14^+)	1331	100	0.13(1)	94(7)	2.43(9)	0.34(1)
4494	(15^+)	1316	100	0.08(1)	140(17)	3.0(2)	0.41(3)
5615	(16^+)	1517	100	< 0.23	> 24	> 1.20	> 0.17
5964	(17^+)	1470	100	< 0.20	> 32	> 1.37	> 0.20

a: Adopted lifetime
b: Using K = 3 at negative parity and K = 4 at positive parity

4 Discussion

The structures of the three nuclei considered in this work have been discussed in several previous papers [12–15, 21–24] to which we refer for the general theoretical concepts. The present measurements result in more reliable lifetimes and add new information on the E2 transition strengths in the upper parts of the rotational bands and therefore complement the lifetime (and Coulomb excitation, in ^{74}Se) measurements of their lower members. From the adopted lifetimes and branching ratios, we deduced the experimental B(E2) values and transitional quadrupole moments $|Q_t|$ listed in Table 2b, 3b and 4b, according to [32]

$$B(E2, I \to I-2) = (5/16\pi)\ e^2\ Q_t^2\ |\langle IK20|I-2\ K\rangle|^2, \tag{3}$$

with

$$|Q_t| = (3/\sqrt{5}\pi)\ Z\ R^2\ (|\beta_2| + 0.16\ \beta_2^2), \tag{4}$$

in second order of the deformation parameter β_2. For the nuclear radius we used $R = 1.2fm\ A^{1/3}$. All experimental

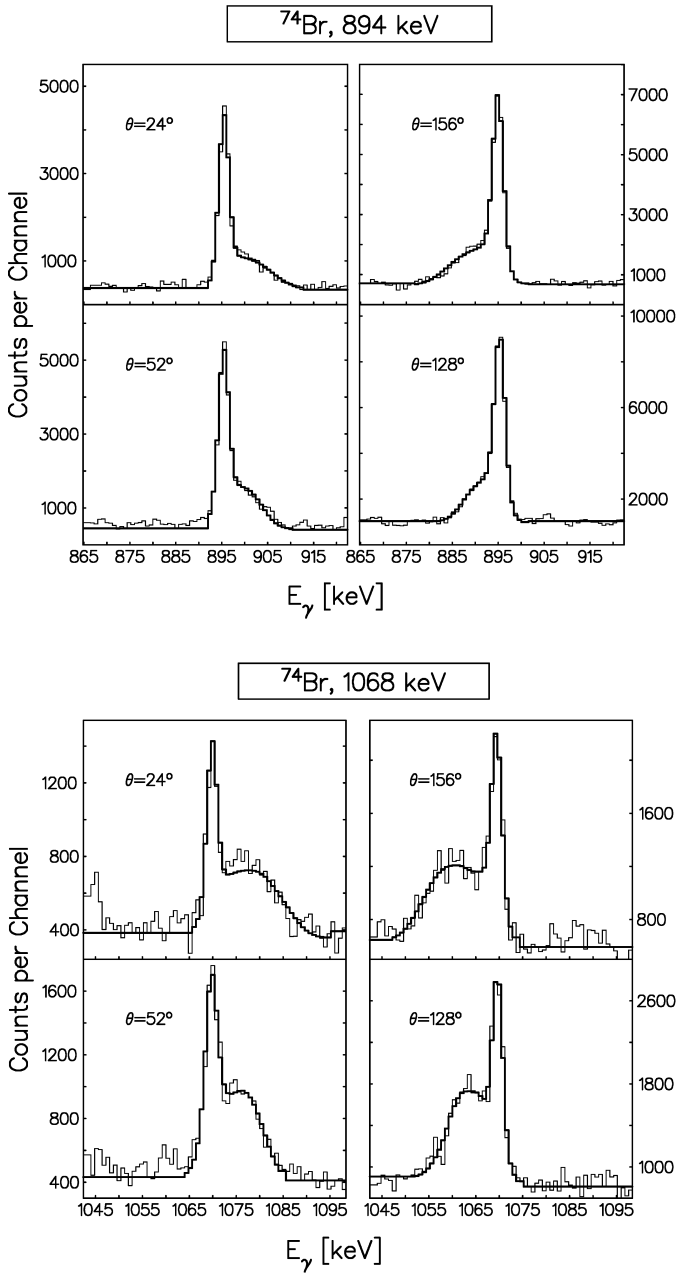

Fig. 8. Measured and fitted lineshapes of the 894 keV transition (top) and the 1068 keV transition (bottom) in ^{74}Br

values of $|Q_t|$ and $|\beta_2|$ were evaluated according to this prescription. As the Cranked Shell Model (CSM) calculations predict non-axial deformations, with the triaxiality parameter γ changing as function of spin, parity and particle number [1], the results of the CSM calculations were transformed into $|Q_t|$ values using the relation [32]

$$Q_t(\beta_2,\gamma) = \sqrt{\frac{12}{5\pi}} ZR^2[\beta_2 \cos(\gamma + 30^o) + \sqrt{\frac{5}{48\pi}}\beta_2^2(\cos^2\gamma - \cos^2(\gamma + 60^o))] \quad (5)$$

^{74}Se: The variation of the transitional quadrupole moments $|Q_t|$ of the yrast band in this nucleus obtained from the adopted lifetimes is displayed in Fig. 9a. Starting at the value $|Q_t| \approx 1.9$ eb for spin I = 2 and 4, one notes an increase to $|Q_t| \approx 2.8$–3.0 eb at spin 6 - 12 and again a decrease to $|Q_t| \approx 2.0$ eb for spin I = 14 and 16. Cranked shell model calculations in this nucleus using a Woods-Saxon single-particle potential and monopole pairing have been recently performed by Döring et al. [14]. The calculated total Routhian surfaces (TRS) of this band predict, at rotational frequency $\hbar\omega \leq 0.807$ MeV, rather well defined potential minima in β_2, but not in the triaxiality parameter γ. This γ-softness even leads to two coexistent shapes at several frequencies. According to the calculations, the deepest minimum develops from $(\beta_2, \gamma) =$ (0.23, -60°) at $\hbar\omega = 0$ MeV to (0.32, -15°) at 0.30 MeV, (0.34, +15°) at 0.40 MeV, (0.30, +30°) at 0.605 MeV to (0.30, +40°) at $\hbar\omega = 0.807$ MeV, i.e. the shape has rather small variations of β_2, but develops from oblate to prolate and finally to non-collective triaxial collectivity ($\gamma > 0$). On the basis of these predictions, we have estimated the $|Q_t(\beta_2,\gamma)|$-values according to (5) and inserted them into Fig. 9a. The agreement is satisfactory. The average quadrupole deformation at spin 8 to 16 would be $|\beta_2| = 0.39(3)$ in the limit of axial rotation.

^{73}Se: The variation of transitional quadrupole moments with spin found by Mukherjee et al. [12] and in the present work is illustrated in Fig. 9b, at positive parity. The structure of this band and of the negative parity yrast band have been interpreted by Kaplan et al. [22] with the Cranked Shell Model and the Decoupled Rotor Model. The calculated TRS of both 1qp neutron bands again indicate "a great deal of γ-softness and a number of competing minima for this nucleus", however, with rather stable $\beta_2 \approx 0.3$. The authors pointed out that no stabilizing effect of the γ-soft even-even core by the odd proton (as observed e.g. in ^{73}Br) occurs in ^{73}Se and that consequently the shape coexistence at low spins found in the even isotopes ^{70,72,74}Se [6,14,16] should persist in ^{73}Se. Indications for oblate deformation at positive parity and for prolate deformation at negative parity have been discussed by Seiffert et al. [21].

^{74}Br: The short lifetimes given in Table 4a complement the values obtained by Döring et al. [14] for spins I < 12, via the recoil distance technique. The yrast bands at positive and negative parity are built upon the 14 keV $4^{(+)}$ and 86 keV (3^-) states and are displayed in Fig. 3c up to the 5964 keV (17^+) and 4908 keV (15^-) level, respectively. Both bands show Δ I = 1 and Δ I = 2 transitions in their lower parts, but only stretched E2 transitions above spin $11^{(-)}$ and (12^+). From Hartree-Fock-Bogoliubov cranking calculations using a Woods-Saxon single-particle potential, Holcomb et al. [15] and Döring et al. [24] obtained total Routhian surfaces (TRS) at rotational energy $\hbar\omega =$ 0.30 MeV. These TRS predict rather stable prolate minima in the (β_2, γ) plane at (0.33, -4°) for the $K^\pi = 4^+$ band, and (0.35, -1°) for the $K^\pi = 3^-$ band, respectively, which are the presumed band heads of the structures discussed in the present work. At this large prolate defor-

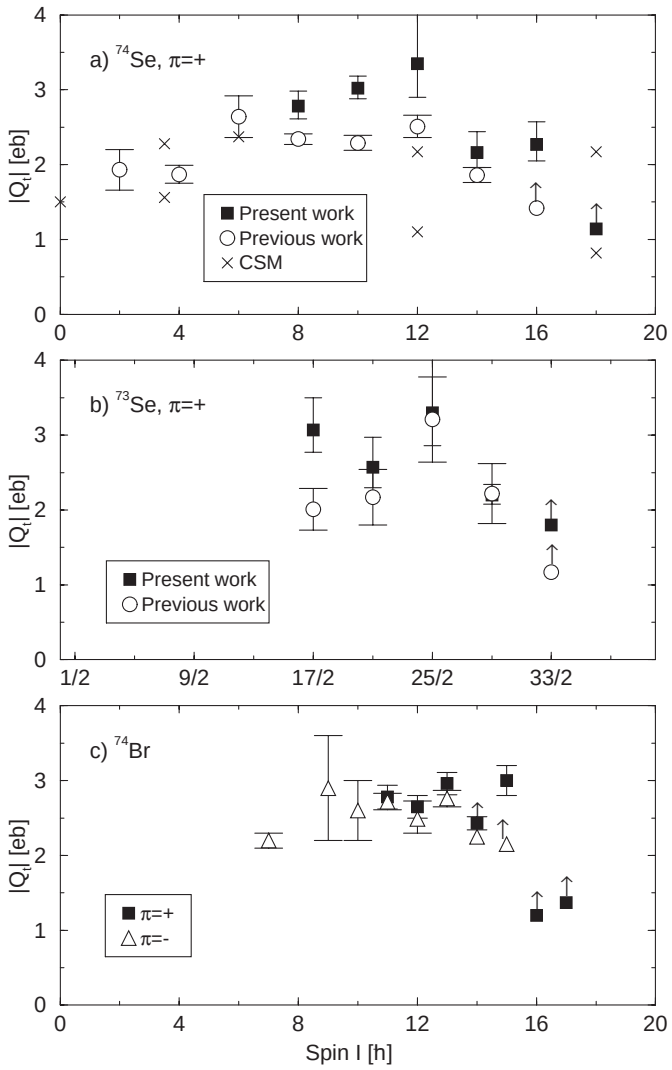

Fig. 9. Measured transitional quadrupole moments $|Q_t|$ (a) in the positive-parity band in ^{74}Se (present and previous [23] work) together with estimates derived from the Cranked Shell Model calculation [14]; (b) in the positive-parity yrast band in ^{73}Se (present and previous [12] work); (c) in the K = 4^+ and 3^- 2qp-bands of ^{74}Br (present and previous [15] work)

mation, the most likely two-quasiparticle Nilsson configuration at $K^\pi = 4^+$ is $\{\pi[431]3/2^+ \otimes \nu[422]5/2^+\}$, with parallel Nilsson projection numbers Ω_π and Ω_ν for the quasi-proton and quasi-neutron, $K = \Omega_\pi + \Omega_\nu = 4$. The magnetic moment of the isomeric band head is, indeed, in agreement with this assignment [24]. According to Döring et al. [24], the negative parity yrast band has most likely a $\{\pi[310]1/2^- \otimes \nu[422]5/2^+\}$ 2qp structure with $K = \Omega_\pi + \Omega_\nu = 3$.

If we use the measured lifetimes and branching ratios for the Δ I = 2 transitions, we arrive at B(E2)'s, transitional quadrupole moments $|Q_t|$ and deformation parameters $|\beta_2|$ listed in Table 4b and displayed in Fig. 9c. Our lifetime measurements give slightly larger quadrupole deformations of $|\beta_2| = 0.37$ than the calculated TRS of $|\beta_2| = 0.33$. However, the average quadrupole moment at negative parity and spin I > 11, $|Q_t| = 2.65(11)$ eb [15], compares well with the figure $|Q_t| = 2.5(2)$ eb measured at lower spin in this band. The same is true at positive parity, where we find $|Q_t| = 2.76(12)$ eb at spin I > 11, to be compared with $|Q_t| = 2.9(1)$ eb at lower spins [15]. In agreement with the TRS calculations, we conclude that both two-quasiparticle configurations stabilize the prolate shape at a constant and large deformation of $\beta_2 = 0.37(1)$ in both bands and block any band crossings due to spin alignments, at least up to about 4.5 MeV excitation. Very recently, Garcia-Bermudez et al. [33] reported on the measurement of ps lifetimes and a staggering of B(M1) values in these two bands below spin $9\hbar$. The authors assigned this staggering to a signature inversion, which is possibly due to the interaction of the 2qp part of the wavefunction with the rotational motion.

5 Conclusions

The present careful DSA experiment using a γ-ray array of high efficiency and solid angle produced Doppler broadened lineshapes of very good counting statistics at several angles when gates were set on transitions lower in the bands. The analysis of these lineshapes led to consistent lifetime values, within better than 10%, at the various detector angles, if the direct sidefeeding time was fixed. Simultaneous fits of the level lifetimes and sidefeeding times still gave consistent results although with much larger uncertainties due to the strong correlation between level lifetime and sidefeeding time. However, the deduced sidefeeding times in ^{74}Se and ^{73}Se agree nicely with the results of Monte-Carlo simulations of the full γ-deexcitation process and therefore give confidence into the calculated sidefeeding times used in the final analysis.

Unfortunately, the gain in counting statistics in the present experiment was partially counteracted by the high Compton continua arising from the fact that the close detector geometry did not allow us to use the BGO shields for Compton suppression in the cluster detectors. The resulting background prevented us from setting clean gates on discrete high-lying feeder transitions at 1.2 - 1.7 MeV and to avoid in this manner the sidefeeding problem altogether.

Concerning the new insights into the structure of these rotational bands, the most important finding is the constant and large (prolate) deformation of $\beta_2 = 0.37(1)$ in the $K^\pi = 3^{(-)}$ and (4^+) bands in ^{74}Br.

The experiments described in this work have been carried out at the Max-Planck-Institut für Kernphysik, Heidelberg. The authors are most grateful to Dr. Repnow and the accelerator crew for their excellent cooperation. The help of Dr. J. Eberth and Dr. H. G. Thomas in setting up the cluster cube array is very much appreciated. One of us, F.C., acknowledges support from Colciencias, Bogotá. The EUROBALL project is being funded by Deutsches Bundesministerium für Bildung, Wissenschaft, Forschung und Technologie (BMBF), Bonn.

References

1. W. Nazarewicz et al., Nucl. Phys. **A435** (1985) 397; W. Nazarewicz and T. Werner, in "Nuclear Structure in the Zirconium Region", R. A. Meyer, J. Eberth, K. Sistemich, Eds., (Springer, Berlin, 1988) p. 272
2. C. J. Lister et al., Phys. Rev. **C28** (1983) 2127
3. C. Thibault et al., Phys. Rev. **C23** (1981) 2720
4. D. R. de la Fosse et al., Phys. Rev. Lett. **78** (1997) 614; D. G. Sarantites et al., Phys. Rev. **C57** (1998) R1; P. J. Gadnall et al., Z. Phys. **A358** (1997) 257
5. J. M. Wiosna, et. al., Phys. Lett. **B200** (1988) 255
6. J. Heese et al., Z. Phys. **A325** (1986) 45
7. H. P. Hellmeister et al., Phys. Rev. **C17** (1978) 2113; Phys. Lett. **85B** (1979) 34
8. B. Wörmann et al., Nucl. Phys. **A431** (1984) 170
9. C. J. Gross et al., Nucl. Phys. **A501** (1989) 367
10. W. Fieber et al., Z. Phys. **A332** (1989) 363
11. H. Schnare et al., Phys. Rev. Lett. **82** (1999) 4408
12. G. Mukherjee et al., Z. Phys. **A359** (1997) 111; G. Mukherjee, private communication
13. J. Adam et al., Z. Phys. **A332** (1989) 143
14. J. Döring et al., Phys. Rev. **C57** (1998) 2912
15. J. W. Holcomb et al., Phys. Rev. **C43** (1991) 470
16. K. P. Lieb and J. J. Kolata, Phys. Rev. **C15** (1977) 937
17. F. Cristancho et al., Nucl. Phys. **A501** (1989) 118
18. A. Harder et al., Phys. Rev. **C55** (1997) 1780
19. J. Eberth et al., Nucl. Instr. Meth. **A369** (1996) 135
20. J. Eberth et al., Prog. Part. Nucl. Phys. **38** (1997) 29; S. Skoda et al., Phys. Rev. **C58** (1998) R5
21. B. Seiffert et al., Z. Phys. **A340** (1991) 141; A. Dewald et al., Z. Phys. **A326** (1987) 509
22. M. S. Kaplan et al., Phys. Rev. **C44** (1991) 668
23. P. D. Cottle et al., Phys. Rev. **C42** (1990) 1254
24. J. Döring et al., Phys. Rev. **C47** (1993) 2560
25. G. Winter, programs DESASTOP, DOPPIDIF, Rossendorf (1983), unpublished; G. Winter, Nucl. Instr. Meth. **214** (1983) 537
26. J. Lindhard, M. Scharff, H. E. Schiøtt, Mat. Fys. Medd. Dan. Vid. Selsk. **36**, no. 10 (1968)
27. M. Halbert et al., Nucl. Phys. **A259** (1976) 496
28. R. B. Piercey et al., Phys. Rev. **C19** (1979) 1344
29. F. Cristancho and K. P. Lieb, Nucl. Phys. **A480** (1988) 353; Nucl. Phys. **A534** (1991) 518
30. A. Gavron, Phys. Rev. **C21** (1980) 230
31. E. Galindo and F. Cristancho, in "Instrumentation in Elementary Particle Physics", G. Herrera Corral, M. Sosa Aquino, Eds. (American Institute of Physics, Woodbury, 1998) p. 387
32. Aa. Bohr, B. R. Mottelson, *Nuclear Structure*, Vol. II (Benjamin, New York, 1975)
33. G. Garcia-Bermudez et al., Phys. Rev. **C59**, (1999) 1999, Phys. Rev. **C23** (1981) 2024